THE ASTROPHYSICAL JOURNAL, 524:L133–L137, 1999 October 20

THE RADIAL AND ANGULAR VARIATION OF THE ELECTRON DENSITY IN THE SOLAR CORONA

P. T. GALLAGHER, M. MATHIOUDAKIS, AND F. P. KEENAN
Department of Pure and Applied Physics, The Queen's University of Belfast, Belfast, BT7 1NN, Northern Ireland
K. J. H. PHILLIPS
Space Science Department, Rutherford Appleton Laboratory, Chilton, Didcot, Oxon, OX11 0QX, England, UK
AND
K. TSINGANOS
Department of Physics, University of Crete, P.O. Box 2208, GR-71003, Heraklion, Crete, Greece
Received 1999 June 11; accepted 1999 August 16; published 1999 September 17

ABSTRACT

We derive, for the first time, electron densities as a function of both radius (R) and position angle (θ) for the southwest quadrant of the off-limb corona, using the density-sensitive Si IX λ349.9/λ341.9 and Si X λ356.0/λ347.7 extreme-ultraviolet line ratios. The observations were made with the coronal diagnostic spectrometer on board the *Solar and Heliospheric Observatory* over the ranges of $1.00\ R_\odot < R < 1.20\ R_\odot$ and $180° < \theta < 270°$. Within the south polar coronal hole, the density varies from 2.3×10^8 cm^{-3} at $1.0\ R_\odot$ to 8.3×10^7 cm^{-3} at $1.20\ R_\odot$, while at the equator, the density varies from 6.3×10^8 cm^{-3} at $1.0\ R_\odot$ to 1.6×10^8 cm^{-3} at $1.20\ R_\odot$. The density falloff with height is therefore faster in the equatorial region. We also find that electron densities are, on average, a factor of 2.7 larger in the equatorial regions than in the polar coronal hole at a given radial distance. Finally, we find remarkable agreement between our measured densities as a function of radius and position angle and those predicted by a recent analytic MHD model of the solar wind, strongly supporting its basic premises.

Subject headings: MHD — solar wind — Sun: corona — Sun: UV radiation — techniques: spectroscopic

1. INTRODUCTION

Extensive observational and theoretical studies of the heliosphere over the past 30 years have revealed that the low-speed solar wind originates from low-latitude, closed-field regions, whereas the high-speed solar wind emanates from coronal holes where the field lines are open (Feldman et al. 1996; Hassler et al. 1999). This expanding solar corona has been modeled recently, either via numerical simulations, with an emphasis on the effects of heat and momentum addition (Wang et al. 1998; Holzer & Leer 1980; Leer & Holzer 1980), or via self-consistent analytical MHD solutions, with an emphasis on the heliographic latitude dependence of the density, wind speed, magnetic field, heating, etc. (Lima, Priest, & Tsinganos 1997). These models produce velocity, temperature, and density profiles as a function of the solar radius and polar angle. An accurate estimate of the electron density distribution in the solar corona is therefore important not just for the corona itself but also for the origin of the solar wind. For example, Wang et al. (1998) have shown that the inclusion of momentum addition in the MHD equations causes significant differences to occur in the velocity and density distributions of the lower corona. Despite difficulties due to the weak line emission, accurate density variations as a function of height have been determined above the coronal holes using the intensity ratios of density-sensitive extreme-ultraviolet (EUV) lines (Doschek et al. 1997). Doyle et al. (1999a) and Doyle, Teriaca, & Banerjee (1999b) have extended this work into the heliosphere, and they have shown that the electron density drops from a value of 10^8 cm^{-3} at the solar limb to a few times 10^3 cm^{-3} at $8\ R_\odot$.

In this Letter, we use Si IX and Si X density-sensitive EUV line ratios to examine the dependence of the electron density as a function of the position angle above the southwest limb. The derived densities from the *Solar and Heliospheric Observatory* (*SOHO*) coronal diagnostic spectrometer (CDS) observations during 1998 are compared with an analytical MHD model of the solar wind, and they are found to be in good agreement.

2. OBSERVATIONS AND DATA REDUCTION

The *SOHO*/CDS instrument consists of the normal-incidence spectrometer (NIS) and the grazing-incidence spectrometer (GIS) operating in the EUV spectral region (151–785 Å). CDS has the capability to form images of the solar atmosphere at particular spectral lines by moving an image of the Sun across the entrance slit with a scan mirror. The NIS used for the current observations is a stigmatic spectrometer with a long entrance slit, with images being formed by moving the solar image across the slit by a scan mirror. The spectral ranges of the NIS (308–381 and 513–633 Å) include lines that are produced over a large temperature range.

The southwest quadrant of the solar corona was observed with NIS between 11:19 and 19:45 UT on 1998 February 28 and between 06:27 and 9:15 UT on March 1. During the observations, the CDS scan mirror was moved so that the solar images were moved 60 times stepwise across the 4×240 arcsec^2 entrance slit so that a 240×240 arcsec^2 area on the Sun was covered. An exposure time of 70 s was used in each slit position. Figure 1 shows a full-Sun *SOHO* EUV Imaging Telescope (EIT) image in the region of Fe XII λ195, with the areas of the CDS rasters indicated. The (EIT) image was taken on 1998 February 26.

Using standard CDS software, the data were first corrected for cosmic-ray events and CCD readout bias and then flat-fielded before the final calibration step was performed to convert the raw data from analog-to-digital conversion units into absolute units (photons cm^{-2} s^{-1} arcsec^{-2}). A further correction, allowing for the fact that the dispersion axes of the NIS spectra are slanted relative to the CCD detector (x, y)-axes, was applied using standard CDS tilt-correction routines (see Gallagher et al. 1998 for further details).

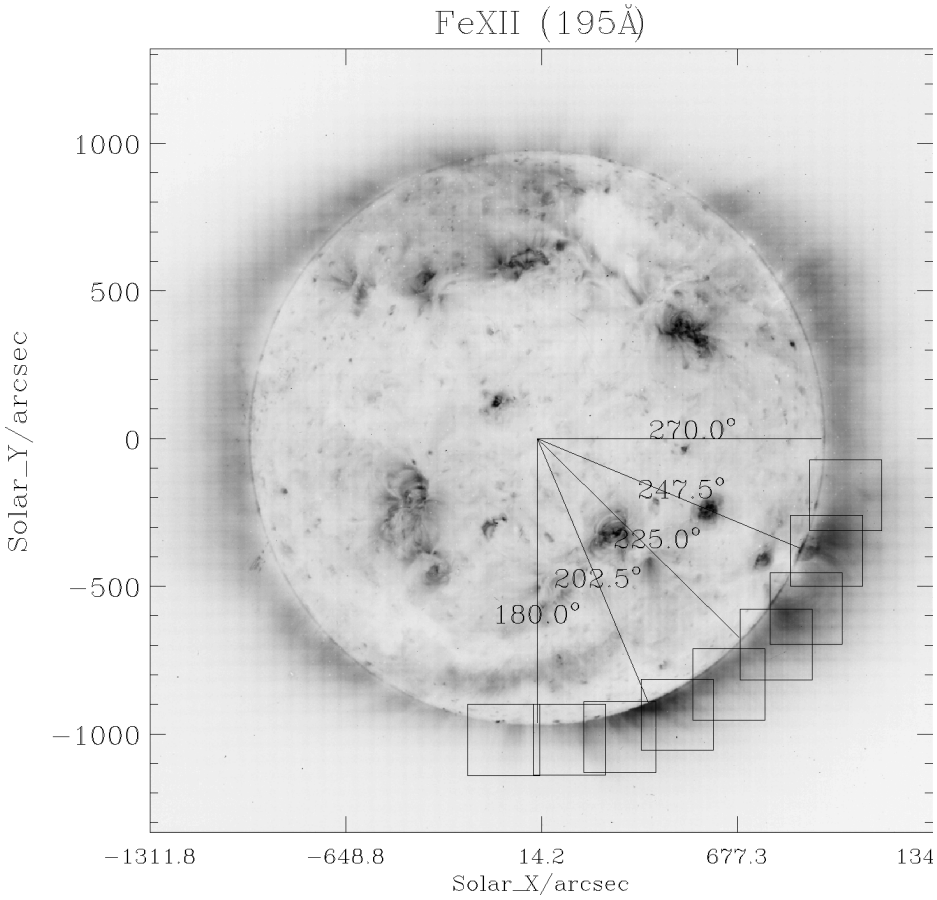

FIG. 1.—Full Sun EIT image in Fe XII λ195 taken on 1998 February 26, together with the nine CDS raster regions studied

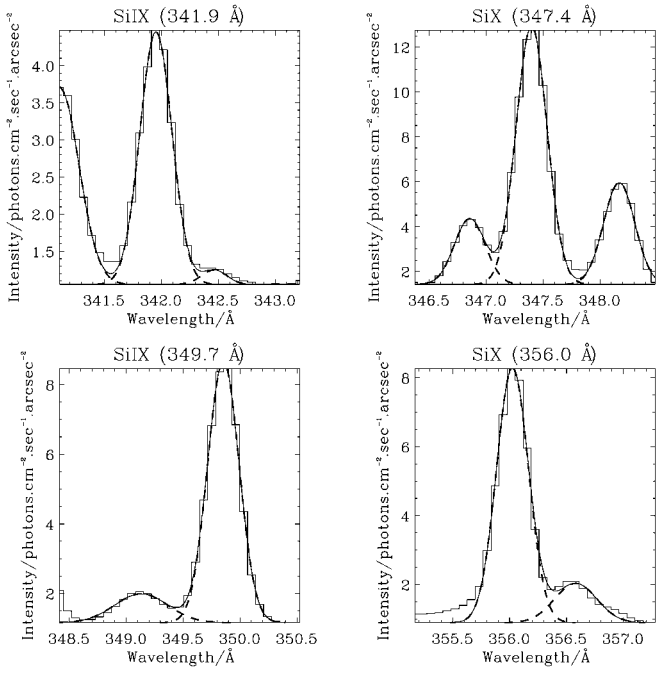

FIG. 2.—The four NIS data windows from which the lines Si IX λ341.9, Si IX λ349.8, Si X λ347.4, and Si X λ356.0 were extracted. The Gaussian and background fits to the raw spectrum are also shown.

Data for the Si IX and Si X lines were extracted from 12 regions in each CDS raster. The rasters were divided into four zones in the radial direction between $1.00\ R_\odot < R < 1.05\ R_\odot$, $1.05\ R_\odot < R < 1.10\ R_\odot$, $1.10\ R_\odot < R < 1.15\ R_\odot$, and $1.15\ R_\odot < R < 1.20\ R_\odot$. Each of these zones was then subdivided into an additional three in the latitudinal direction. An average line profile was then extracted from each region, and the line intensities estimated from Gaussian fits to the data. Figure 2 gives an example of the line profiles studied, together with the Gaussian and background fits used, and shows that the lines are free from blends, and hence line intensity ratios should be reliable.

3. DIAGNOSTIC LINE RATIOS

We have used the Si IX λ349.9/λ341.9 and Si X λ356.0/λ347.7 line ratios to derive values of electron density, in conjunction with the calculations of Doyle et al. (1999a) and Keenan et al. (1999), respectively. The theoretical ratios presented by these authors have been derived using electron collisional excitation rates calculated with the ***R***-matrix code; they are expected to have very high accuracy (better than 20%). However, we note that the line ratios are very similar to those calculated from the CHIANTI database (Landi et al. 1999), and in addition the adoption of the latter would not affect the results or discussion presented in this Letter.

Electron densities have been deduced from the theoretical

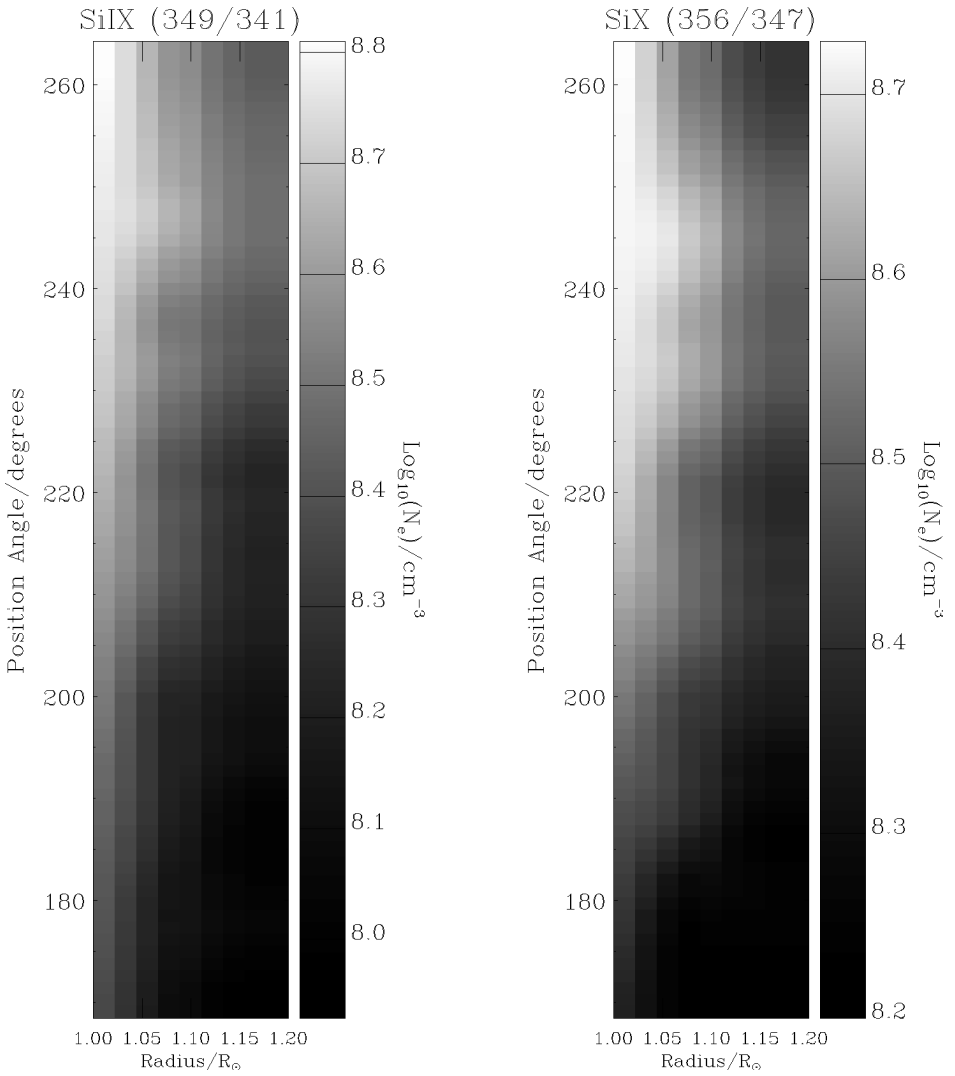

FIG. 3.—The electron density as a function of radius and position angle from Si IX λ349.8/λ341.9 and Si X λ356.0/λ347.4. The color bar to the right of each image indicates the density scale.

diagnostics on the assumption that the electron temperature is that of maximum fractional abundance in ionization equilibrium, which is $T_{\max} \simeq 1.3 \times 10^6$ K for both Si IX and Si X (Mazzotta et al. 1998). However, we note that the derived electron densities are almost independent of T_e because of the low-temperature sensitivity of the theoretical line ratios. For example, changing the adopted value of $T_{\max}$ by a factor of 2 leads to less than a 0.1 dex variation in the derived density (Doyle et al. 1999a).

4. RESULTS AND DISCUSSION

Figure 3 shows the logarithm of the electron density ($\log N_e$) as a function of radial distance (R) and position angle (θ) for the southwest quadrant of the solar corona. The data have also been rebinned to enhance the visibility of faint coronal features. As is evident from Figure 3, the Si X λ356.0/λ347.4 densities are consistent with the Si IX λ349.7/λ341.9 values, considering that the former is a factor of 3 less sensitive in the range $8.2 < \log N_e < 10.0$ and is insensitive to density for $\log N_e < 8.2$. It should also be noted that the derived density values are only accurate to ± 0.2 dex as a result of uncertainties in the atomic data and derived ratios and, less importantly, as a result of line-of-sight effects (see Cranmer et al. 1999 and Li et al. 1998 for a further discussion of line-of-sight effects).

The electron density in the radial direction within the coronal hole varies from 2.3×10^8 cm^{-3} at the limb to 8.3×10^7 cm^{-3} at 1.20 $R_\odot$. This variation is in good agreement with the recent Si IX and Si VIII results of Doyle et al. (1999a, 1999b), Fludra et al. (1999a), and Fludra, Del Zanna, & Bromage (1999b). The equatorial density varies from 6.3×10^8 cm^{-3} at the limb to 1.6×10^8 cm^{-3} at 1.20 $R_\odot$. Electron densities in equatorial regions are, on average, a factor of 2.7 higher than in the polar coronal hole at a given radial distance. The increased densities at $\theta \sim 250°$ and 235° are associated with the two active regions on the limb (see Fig. 1). Note that the density gradient, measured by $N_e(r = 1.0\ R_\odot)/N_e(r = 1.2\ R_\odot)$, is greater for the equatorial region (3.8) than for the south polar coronal hole (2.8).

We have also compared the heliolatitudinal density profile with the HD solar wind model of Lima & Priest (1993) and the corresponding MHD solar wind model of Lima et al. (1997). In these models, the magnetohydrodynamical equations describing the dynamical interaction of an inviscid, compressible, and highly conducting plasma with an axially symmetric mag-

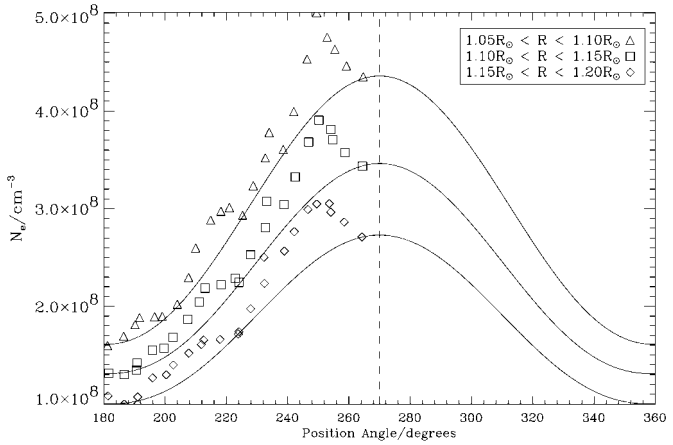

FIG. 4.—Comparison of electron densities derived in this work with the models of Lima & Priest (1993) and Lima et al. (1997). In each case, the parameters δ and ϵ from eq. (1) were evaluated using a χ^2 minimization routine. The values of δ and ϵ for each density profile are given in Table 1.

netic field are solved using a technique involving the nonlinear separation of variables. The analysis gives three dimensionless parameters, δ, ϵ, and μ, that control the degree of the heliolatitudinal anisotropy of the distribution of the density, bulk flow speed, magnetic flux, etc. The solution that expresses the radial and heliographic latitude dependence of the density is as follows:

$$\rho(R, \theta) = \frac{\rho_0}{YR^2}(1 + \delta \sin^{2\epsilon} \theta), \quad (1)$$

where $Y(R)$ gives the radial dependence of the solar wind velocity, δ relates the density at the equator to the density at the poles and can be expressed as

$$\delta = \frac{\rho(R, 270°)}{\rho(R, 180°)} - 1, \quad (2)$$

and ϵ controls the width of the density (and velocity) profile. The higher the value of δ, the more the density distribution deviates from the spherically symmetric case, while the higher the value of ϵ, the narrower the density profile becomes at the equator.

To compare the angular density variation derived using CDS with the model of Lima at al. (1997), three density profiles ranging from 180° to 270° were extracted over three radial intervals. These are given in Figure 4. The model of Lima at al. (1997) may only be reliably applied to the quiet corona near solar minimum, so electron densities derived within active regions were neglected when comparing our observations with theory. The positions and angular extents of any active regions observed during the CDS observations were estimated using the EIT image given in Figure 1. Densities derived within the active regions were neglected during the fitting procedure. The optimum values of the parameters δ and ϵ were evaluated by fitting the selected quiet coronal density profiles with equation (1). These values are given in Table 1. The best fits to the heliolatitudinal Si IX density profiles for the three radial distances, 1.05 $R_\odot < R < 1.10$ $R_\odot$, 1.10 $R_\odot < R < 1.15$ $R_\odot$, and 1.15 $R_\odot < R < 1.20$ $R_\odot$, are shown as solid lines in Figure 4. As can be seen, there is good agreement between the model and the quiet coronal density profiles.

TABLE 1

MODEL PARAMETERS USED TO FIT THE HELIOLATITUDINAL DENSITY PROFILES

Radial Distance	δ	ϵ
1.05 $R_\odot < R < 1.10$ $R_\odot$	1.74	1.20
1.10 $R_\odot < R < 1.15$ $R_\odot$	1.65	1.18
1.15 $R_\odot < R < 1.20$ $R_\odot$	1.70	1.09

The derived values of δ from the present 1998 CDS observations, reflecting a factor of 2.7 increase in the density at the equator relative to the polar coronal hole, are similar to the value of δ derived from the 1995 *Ulysses* observations (Phillips et al. 1995; Lima et al. 1997). However, the derived values of ϵ from the CDS observations are considerably lower than the corresponding values of ϵ from the 1995 *Ulysses* observations. Thus, while the value of the parameter δ seems to be relatively independent of the phase of the solar cycle, the value of the parameter ϵ is higher around solar minimum and drops considerably as solar maximum is approached—for large values of ϵ, the density as a function of θ has a narrow profile, typical of solar minimum, while small values produce a more uniform profile, characteristic of solar maximum. It is interesting to note that a similar increase of ϵ from solar maximum to solar minimum appears in an interpretation of interplanetary scintillation observations from the previous solar cycles (Rickett & Coles 1991).

P. T. G. is grateful to the Department of Education for Northern Ireland and the Rutherford Appleton Laboratory for financial support. This work was supported by PPARC, the Leverhulme Trust, and the Nuffield Foundation (NUF-NAL).

REFERENCES

Cranmer, S. R., et al. 1999, ApJ, 511, 481
Doschek, G. A., Warren, H. P., Laming, J. M., Mariska, J. T., Wilhelm, K., Lemaire, P., Schuhle, U., & Moran, T. G. 1997, ApJ, 482, L109
Doyle, J. G., Keenan, F. P., Ryans, R. S. I., Aggarwal, K. M., & Fludra, A. 1999a, Sol. Phys., in press
Doyle, J. G., Teriaca, L., & Banerjee, D. 1999b, A&A, in press
Feldman, W. C., Phillips, J. L., Barraclough, B. L., & Hammond, C. M. 1996, in Solar and Astrophysical Magnetohydrodynamic Flows, ed. K. C. Tsinganos (NATO ASI Ser. C, 481; Dordrecht: Kluwer), 265
Fludra, A., Del Zanna, G., Alexander, D., & Bromage, B. J. I. 1999a, J. Geophys. Res., in press
Fludra, A., Del Zanna, G., & Bromage, B. J. I. 1999b, Space Sci. Rev., in press
Gallagher, P. T., Phillips, K. J. H., Harra-Murnion, L. K., & Keenan, F. P. 1998, A&A, 335, 733
Hassler, D. M., Dammasch, I. E., Lemaire, P., Brekke, P., Curdt, W., Mason, H. E., Vial, J.-C., & Wilhelm, K. 1999, Science, 283, 810
Holzer, T. E., & Leer, E. 1980, J. Geophys. Res., 85, 4665
Keenan, F. P., Foster-Woods, V. J., O'Shea, E., Thomas, R. J., Brosius, J., Ryans, R. S. I., Zhang, H. L., & Pradhan, A. K. 1999, MNRAS, submitted
Landi, E., Landini, M., Dere, K. P., Young, P. R., & Mason, H. E. 1999, A&AS, 135, 339
Leer, E., & Holzer, T. E. 1980, J. Geophys. Res., 85, 4681
Li, J., Raymond, J. C., Acton, L. W., Kohl, J. L., Romoli, M., & Naletto, G. 1998, ApJ, 506, 431
Lima, J. J. G., & Priest, E. R. 1993, A&A, 268, 641
Lima, J. J. G., Priest, E. R., & Tsinganos, K. 1997, in Fifth *SOHO* Workshop, The Corona and Solar Wind near Minimum Activity, ed. A. Wilson (ESA SP-404; Noordwijk: ESA), 533

Mazzotta, P., Mazzitelli, G., Colafrancesco, S., & Vittorio, N. 1998, A&AS, 133, 403
Phillips, J. L., et al. 1995, Geophys. Res. Lett., 22(23), 3301
Rickett, B. J., & Coles, W. A. 1991, J. Geophys. Res., 96, 1717
Wang, A. H., Wu, S. T., Suess, S. T., & Poletto, G. 1998, J. Geophys. Res., 103, 1913